European Journal of Medicinal Chemistry 83 (2014) 455–465

Contents lists available at ScienceDirect

European Journal of Medicinal Chemistry

journal homepage: http://www.elsevier.com/locate/ejmech

Original article

A new 9-alkyladenine-cyclic methylglyoxal diadduct activates wt- and F508del-cystic fibrosis transmembrane conductance regulator (CFTR) *in vitro* and *in vivo*

Benjamin Boucherle [a, 1], Johanna Bertrand [b, 1], Bruno Maurin [a], Brice-Loïc Renard [a], Antoine Fortuné [a], Brice Tremblier [b], Frédéric Becq [b], Caroline Norez [b], Jean-Luc Décout [a, *]

[a] Université Grenoble Alpes, Joseph Fourier/CNRS, UMR 5063, Département de Pharmacochimie Moléculaire, 470 rue de la Chimie, F-38041 Grenoble, France
[b] Université de Poitiers/CNRS, Laboratoire Signalisation et Transports Ioniques Membranaires, 1 rue Georges Bonnet, F-86022 Poitiers, France

ARTICLE INFO

Article history:
Received 8 February 2014
Received in revised form
12 June 2014
Accepted 13 June 2014
Available online 14 June 2014

Keywords:
Cystic fibrosis
F508del-CFTR
Modulators
Activators
Salivary secretion
Docking
Nucleotide binding domains

ABSTRACT

Cystic fibrosis transmembrane conductance regulator (CFTR) is the main chloride channel present in the apical membrane of epithelial cells and the F508 deletion (F508del-CFTR) in the *CF* gene is the most common cystic fibrosis-causing mutation. In the search for a pharmacotherapy of cystic fibrosis caused by the F508del-CFTR, a bi-therapy could be developed associating a corrector of F508del-CFTR trafficking and an activator of the channel activity of CFTR. Here, we report on the synthesis of 9-alkyladenine derivatives analogues of our previously discovered activator of wt-CFTR and F508del-CFTR, GPact-11a, and the identification of a new activator of these channels, GPact-26a, through various flux assays on human airway epithelial CF and non-CF cell lines and *in vivo* measurement of rat salivary secretion. This study reveals that the possible modifications of the side chain introduced at the *N*9 position of the main pharmacophore are highly limited since only an allyl group can replace the propyl side chain present in GPact-11a to lead to a strong activation of wt-CFTR in CHO cells. Docking simulations of the synthesised compounds and of four described modulators performed using a 3D model of the wt-type CFTR protein suggest five possible binding sites located at the interface of the nucleotide binding domains NBD1/NBD2. However, the docking study did not allow the differentiation between active and non-active compounds.

1. Introduction

The Cystic Fibrosis Transmembrane conductance Regulator (CFTR) protein is a cAMP-regulated chloride channel controlling transepithelial Cl^- transport and belonging to the ATP-binding cassette (ABC) superfamily [1–6]. CFTR is the only one of the numerous members of the ABC superfamily known to function as an ion channel.

The mutations of the *CF* gene encoding CFTR cause the genetic disease cystic fibrosis (CF) [1,4–6] that is the most common lethal autosomal recessive genetic disease in Caucasians (more than 1900 identified mutations, http://www.genet.sickkids.on.ca/cftr). These numerous mutations can be classified according to the fate of the final product into five classes [6]. The F508 deletion (F508del) is the most common cystic fibrosis-causing mutation that induces reduced channel function, early degradation and poor trafficking of modified CFTR protein to the apical membrane of epithelial cells (Class II) [7]. The protein consists of 1480 amino acid residues forming (i) two membrane-spanning domains (MSD1 and MSD2) composed each by six transmembrane helices (TM1 to TM6 and TM7 to TM12) and by intracellular loops (ICLs), (ii) two cytoplasmic nucleotide binding domains (NBD1 and NBD2) and (iii) a large regulatory domain (R). The two NBDs form tightly interacting dimers upon ATP-binding at their interface [8]. ATP-binding and dimerization of the NBDs are coupled to channel opening, whereas ATP hydrolysis at composite site 2 leads to the channel closure. The

Abbreviations: CF, cystic fibrosis; CFTR, cystic fibrosis transmembrane conductance regulator; CHO cells, Chinese hamster ovaries cells; CMGD, cyclic methylglyoxal diadducts; DMTr, 4,4′-dimethoxytrityl; ICL, intracellular loop; MG, methylglyoxal; MSD, membrane-spanning domain; NBD, nucleotide binding domain; TM, transmembrane helice.

* Corresponding author.
E-mail address: jean-luc.decout@ujf-grenoble.fr (J.-L. Décout).

[1] Equal contributions of these authors.

http://dx.doi.org/10.1016/j.ejmech.2014.06.028
0223-5234/

non-canonical ATP-binding site 1 binds nucleotide tightly but is not hydrolytic, suggesting that this site remains closed throughout the gating site and that a limited separation of the NBDs occur [8].

As a large polytopic membrane protein containing disordered regions, intact CFTR has been refractory to efforts to solve a high-resolution structure using X-ray crystallography [9]. Only crystal structures of the wild type and mutated NBD1 [10,11] and NBD2 [12] have been solved, which together with previous modelling studies of the NBD1:NBD2 heterodimer [13,14] have provided the first significant insights into the role that the F508 residue would play in the formation of inter-domain contacts. This role was clearly evidenced by the two first homology models of the whole NBD-MSD assembly, build on the basis of the crystal structure of the bacterial Sav1866 [10,11,15], as the F-508 residue was indeed shown to be located at the interface between NBD1 and ICL4 from MSD2 [16]. These models were assumed to approximate the open form of the channel, at least in the cytoplasmic domains, as both NDB are tightly associated, with ATP bound at their interfaces.

Recent approval of a CF protein modulator, ivacaftor (Kalydeco), in a small group of patients with the G551D mutation has ignited an explosion of interest for other modulators directed at different CFTR mutation classes [17–29]. This Class III mutation results in a channel open probability strongly lower than that of the wild-type channel. One of the major therapeutic strategy in CF aims at developing modulators of CFTR activity and, in the case of F508del, a bi-therapy could be used associating a corrector of F508del-CFTR trafficking and an activator.

In the search for modulators of CFTR, we have recently identified GPact-11a (**1a**) (Fig. 1) as a non-toxic and water-soluble CFTR activator [30]. We showed that GPact-11a activates F508del-CFTR when rescued by correctors including miglustat, in nasal, tracheal, bronchial, pancreatic CF cell lines and in human CF ciliated epithelial cells freshly dissociated from lung samples (iodide efflux, fluorescence imaging and patch-clamp recordings). GPact-11a also stimulates *ex vivo* the colonic chloride secretion (short-circuit current measurements) and increases *in vivo* the salivary secretion in $cftr^{+/+}$ but not in $cftr^{-/-}$ mice [30]. The effects appeared to be selective for CFTR since they are inhibited by $CFTR_{inh}$-172 [31], GlyH-101 [32], glibenclamide and GPinh-5a (**2a**) (Fig. 1), an inhibitor of CFTR that we have identified previously having a structure closely related to the structure of GPact-11a [33] (Fig. 1).

The previously identified activator GPact-11a **1a** and inhibitor GPinh-5a **2a** have been obtained by condensation of two molecules of methylglyoxal (MG) with one molecule of 9-propyladenine and 2′-deoxyadenosine, respectively, leading to cyclic methylglyoxal diadducts (CMGD) [34]. More recently, we also described two 5-pyrimidinols, obtained from prepared CMGD to 2-aminopyridine and 1-aminoisoquinoline, that are able to strongly inhibit the activity of CFTR channels in wt-CFTR CHO cells [35]. The activator GPact-11a and inhibitor GPinh-5a are made of a same heterocyclic core and differ only from the substituent present at the 9-position of the heterocyclic ring which are a propyl chain and a 2-deoxyribosyl substituent, respectively (numbering according to the usual adenine ring numbering, Fig. 1). In these structures, the nature of the 9-substituent appears to be essential for modulating the effects on CFTR and we modified this side chain in the search for new CFTR modulators through delineation of structure–activity relationships.

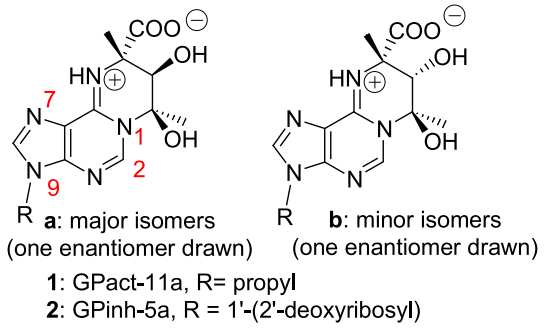

Fig. 1. Structure of the previously identified activator GPact-11a [30] and inhibitor GPinh-5a [33] of wt- and F508del-CFTR channels *in vitro* and *in vivo*.

Here, we report on the synthesis of analogues of GPact-11a and the identification, in the same family, of a new CFTR-activator GPact-26a in CHO cells stably expressing wt-CFTR. This compound showed similar *in vitro* and *in vivo* effects to those of GPact-11a and was also able to activate rescued F508del-CFTR in human airway epithelial CF15 cell line. Since, GPact-26a is able to activate wt-CFTR, we carried out molecular modelling docking simulations using the 3D model published by Mornon et al. [11]. In the search for potential binding sites of discovered activators and inhibitors, we also report here on these simulations that suggests several common possible binding sites shared by activators and inhibitors of the GP-family and located at the key NBD1/NBD2 interface in the protein. These possible targets remain to be related to the observed biological effects through site-directed mutagenesis experiments.

2. Results

2.1. Chemistry

GPact-11a has been prepared by condensation of 9-propyladenine (prepared by alkylation of the nucleic base adenine) and methylglyoxal (MG). Such a condensation led to four isomers of cyclic methylglyoxal diadducts (CMGD) isolated as two racemic mixtures of enantiomers **1a** (GPact-11a) and **1b** (GPact-11b) formed in a 60:40 ratio [34].

In a first approach in the delineation of structure–activity relationships, the chemical modifications in the GPact-11a structure were designed in order to maintain the hydrophobic character of the 9-substituent and the propyl side chain was replaced by different alkyl chains: methyl, ethyl, isopropyl, butyl, allyl, propargyl, benzyl and 3-phenylpropyl groups (Scheme 1). A compound in which the 3-hydroxypropyl group replaces the propyl chain was also prepared in order to evaluate the role of the chain lipophilicity (Scheme 1).

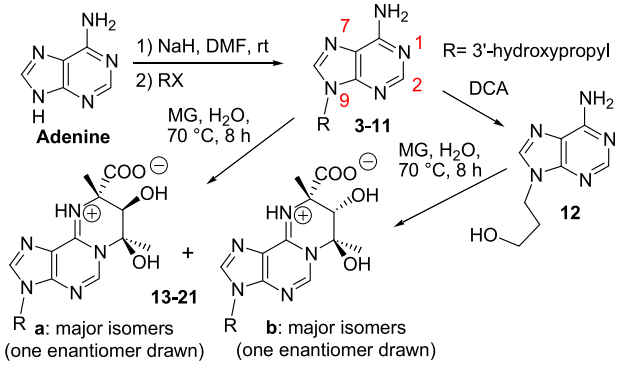

3 and **13a,b**: R= CH_3; **4** and **14a,b**: R= C_2H_5; **5** and **15a,b**: R= isopropyl;
6 and **16a,b**: R= butyl; **7** and **17a,b**: R= allyl; **8** and **18a,b**: R= propargyl;
9 and **19a,b**: R= benzyl; **10** and **20a,b**: R= 3'-phenylpropyl;
11: 3'-(DMTr-oxy)propyl and **21a,b**: R= 3'-hydroxypropyl

Scheme 1. General method used for the preparation of the 9-alkyladenine-cyclic methylglyoxal diadducts.

Previously, we have observed that both mixtures of enantiomers **1a** and **1b** have close EC_{50} on wt-CFTR in CHO cells (^{125}I iodide efflux assay: EC_{50} = 2.1 ± 1.3 and 2.9 ± 0.9 μM, respectively) [30] and thus, in a first approach, the mixtures of major enantiomers **a** of the prepared analogues were isolated and evaluated.

The commercially available 9-methyladenine **3** and 9-ethyladenine **4** were converted to the corresponding CMGD derivatives **13a**,**b** and **14a**,**b** through reaction with MG (Scheme 1). The diasteroisomeric mixtures of enantiomers **13a** and **14a** were isolated by reversed phase chromatography. With the exception of the 3-hydroxypropyl derivative **21a**, the other 9-alkylated CMGD analogues of GPact-11a **15a**–**20a** were prepared from adenine in two steps (Scheme 1) (i) alkylation with the corresponding bromoalkylating reagent in the presence of NaH in DMF for obtaining the 9-alkyladenine derivatives **5**–**10** and (ii) reaction of **5**–**10** with MG in excess. The second step led as previously to four isomers as two racemic mixtures of enantiomers **a** and **b** from which the mixtures **a** were isolated. The 3-hydroxypropyl derivatives **21a** were obtained in four steps (Scheme 1): (i) preparation of the alkylating reagent 3-bromo-1-(4,4′-dimethoxytrityloxy)propane, (ii) alkylation of adenine with this reagent to lead to **11**, (iii) removal of the trityl group in the presence of dichloroacetic acid and (iv) reaction with MG of the deprotected intermediate **12**.

We also tried to synthesise the corresponding CMGD to 7-methyl- and 7-propyl-adenines which have been isolated as minor products in the step of adenine alkylation. Unfortunately the cyclization with MG did not occur probably due to steric hindrance.

2.2. Biological evaluation

A number of methods are currently employed to assess the functional properties of CFTR channels and their response to pharmacological potentiators and correction of the defective CFTR trafficking [36].

First, we examined the effect of the synthesised compounds in CHO cells stably expressing wt-CFTR through a robotic cell-based primary screening assay using radioactive iodide efflux measurements. Because the CFTR channel is permeable to iodide, these measurements are related to the chloride efflux and allow a rapid detection of CFTR channel activation or inhibition.

The synthesised analogues of GPact-11a **13a**–**21a** were evaluated by this iodide efflux technique at a concentration of 100 μM in the presence of forskolin (Fsk) at 1 μM (Fig. 2). Fsk, a terpene derivative of plant origin, activates adenylate cyclase and leads to an intracellular increase of cAMP sufficient to activate the cAMP-dependent protein kinase A (PKA) with the consequent activation of the CFTR. Among the evaluated compounds, only **17a** (GPact-26a) revealed a detectable potentiation of the Fsk effect under the conditions used (Fig. 2).

The cell viability in the presence of **17a** was then evaluated in wt-CFTR CHO cells after 24 h of incubation using the colorimetric MTT assay (reduction of 3-[4,5-dimethylthiazol-2-yl]-2,5-diphenyl tetrazolium in the mitochondria to purple formazan, Fig. 3).

Since **17a** appeared to be non-cytotoxic up to 300 μM concentrations, we determined in a second step the half maximal effective concentration EC_{50} of this compound. The study of the concentration-response effect, in the presence of Fsk (1 μM), showed an EC_{50} of 7.5 ± 1.7 μM (standard error of mean, Fig. 4).

In order to investigate the effects of the corresponding isomers **b**, the mixture **17b** was isolated and the corresponding EC_{50} was measured in a similar experiment with CHO cells. The value obtained was EC_{50} = 2.1 ± 1.2 μM. In regard to the errors calculated from the concentrations of the prepared solutions of **17a** and **17b**, we concluded that there is no major difference of activity between both mixtures of enantiomers **17a** and **17b**. Thus, the major isomers **17a** (GPact-26a) were further studied.

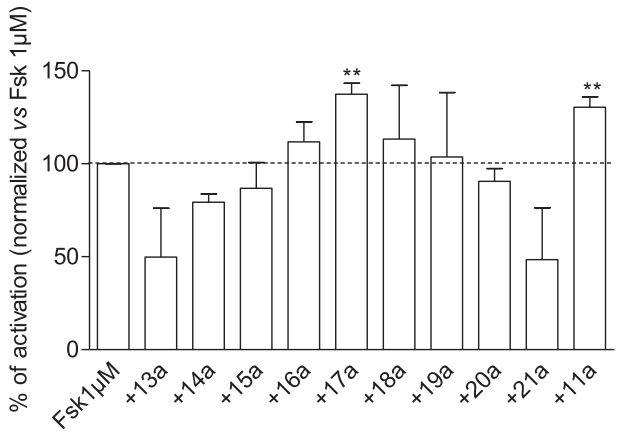

Fig. 2. Effect of the synthesised GPact11a analogues (100 μM) on iodide efflux stimulated by forskolin (Fsk, 1 μM) in wt-CFTR CHO cells. Data are expressed as a percentage of Fsk induced response, $n = 4$ for each condition, $^{**}p < 0.01$.

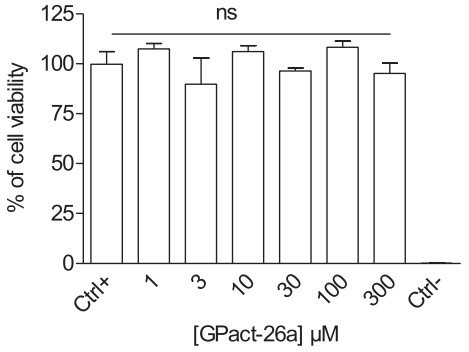

Fig. 3. Viability of wt-CFTR CHO cells in the presence of **17a** (GPact-26a) (24 h) using the colorimetric MTT assay. Ctrl+ corresponds to untreated cells and Ctrl− corresponds to cells private of medium during 24 h.

The slow-response potential-sensitive probe bis-(1,3 diethylthiobarbituric acid)trimethine oxonol ($DiSBAC_2(3)$) can be used to estimate the intracellular chloride concentration change. Increased chloride concentrations results in additional influx of the anionic dye and an increase in cell fluorescence. Thus, GPact-26a was further studied using the single cell fluorescence imaging technique developed with the oxonol ($DiSBAC_2(3)$) probe applied to the human tracheal gland epithelial cell line MM39 (Fig. 5A, B) [37].

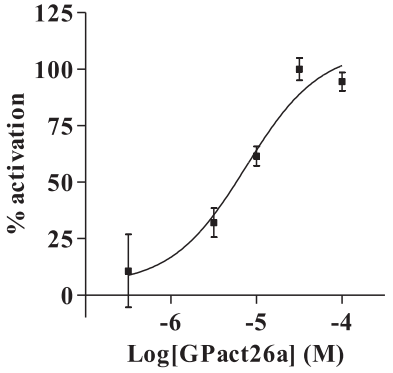

Fig. 4. Evaluation of **17a** (GPact-26a) using the iodide efflux technique in wt-CFTR CHO cells in the presence of Fsk at 1 μM. The half-maximal effective concentration for activation (EC_{50}) was calculated after nonlinear regression of the data.

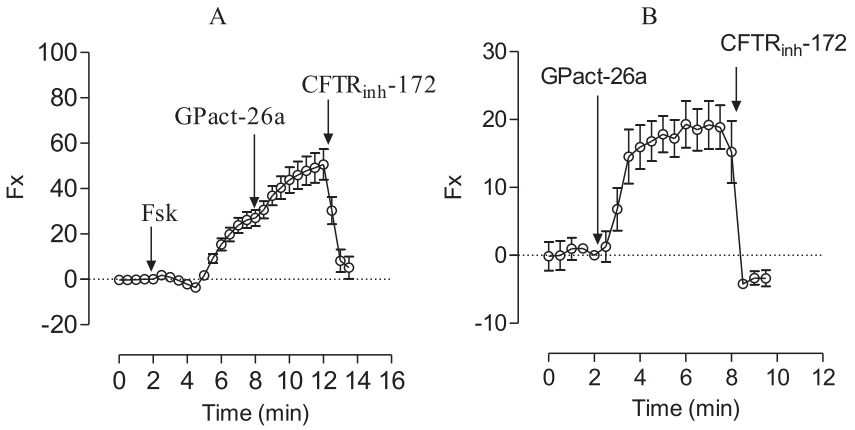

Fig. 5. Functional evaluation of **17a** (GPact-26a) by DISBAC$_2$ assay [37] in human tracheal gland epithelial cells MM39. (A) Example of mean traces showing potentiation of the forskolin (Fsk, 1 μM)-induced activation of CFTR; (B): activation in the absence of Fsk. Data represent the mean (±SEM) of the relative fluorescence collected (F_x) in arbitrary units (λ_{ex} = 535 nm, λ_{em} = 560 nm). CFTRinh-172 at 1 μM concentration was used to inhibit the CFTR activity.

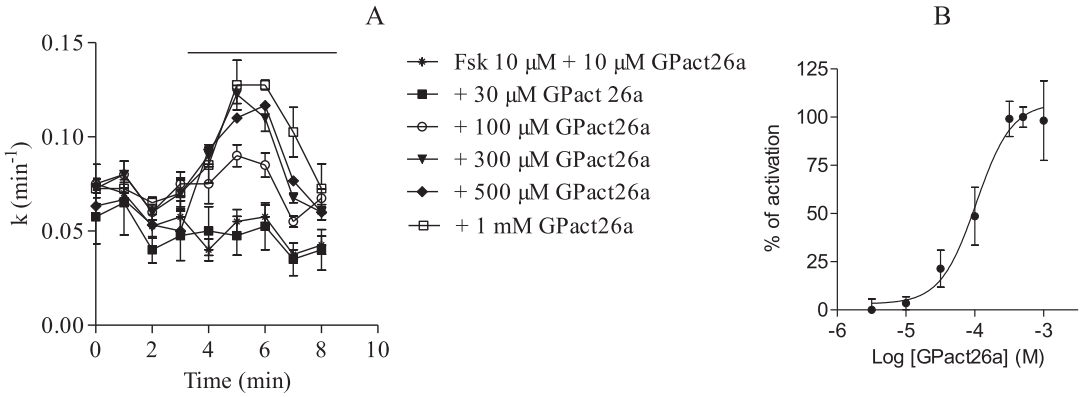

Fig. 6. Evaluation of **17a** (GPact-26a) using the iodide (^{125}I) efflux technique in miglustat-corrected CF15 cells in the presence of Forskolin (Fsk) at 10 μM. (A): Concentration-response time-dependent curves were plotted by measuring the rate of iodide efflux (min^{-1}); (B): The half-maximal effective concentration for activation (EC_{50}) was calculated after nonlinear regression of the data.

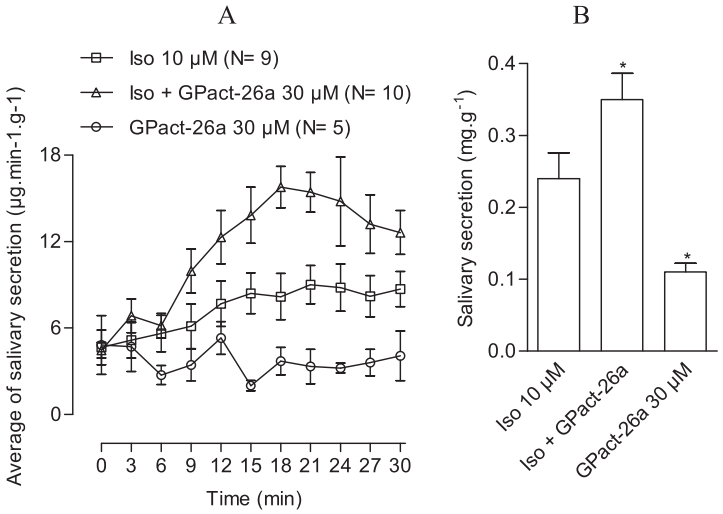

Fig. 7. Evaluation of **17a** (GPact-26a) on rat salivary secretion collected in response to subcutaneous injection. Basal salivary secretion was inhibited by atropine (1 mM) prior to injection of a saline solution containing atropine (1 mM) mixed with isoprenaline (Iso, 10 μM) alone or the mixture isoprenaline + GP-act26a (10 and 30 μM, respectively) or GP-act26a alone (30 μM). (A): The average of salivary secretion was determined in dividing the weight of collected saliva by the time required for collection in min and by the weight of the rat in g; (B): The total saliva secretion was determined by addition of all the samples of saliva collected during the experiment.

We observed that GPact-26a (**17a**) increases the fluorescence in the presence of Fsk at 1 μM confirming its potentiating effect in MM39 cells. This observed Fsk/GPact-26a-induced response was fully inhibited by the previously reported inhibitor $CFTR_{inh}$-172 [31](Fig. 5A). Clearly, these results confirm the wt-CFTR potentiating effect of GPact-26a in human epithelial cells. Moreover, in the absence of Fsk, the fluorescent signal was also increased by GPact-26a alone and fully inhibited by addition of the $CFTR_{inh}$-172 suggesting that GPact-26a (**17a**) is an activator of CFTR and not only a CFTR potentiator in the presence of Fsk (Fig. 5B). The same results have been obtained previously with GPact-11a (**1a**) [30].

To study the effect of GPact-26a on F508del-CFTR, we determined its effect on miglustat-corrected human airway epithelial cell line CF15 by the iodide efflux technique. This compound induced a concentration-dependent potentiation of iodide efflux (Fig. 6A) with an $EC_{50} = 104 \pm 2$ μM in the presence of forskolin at 10 μM as shown in Fig. 6B.

Measurement of salivary secretion (weight of saliva) is a good non-invasive technique to study fluid and electrolyte secretion *in vivo* [30,38]. Saliva is secreted in response to cholinergic and adrenergic agonists by the coordinated action and regulation of multiple water and ion transporters and ionic channels. Fluid and electrolyte transport is driven by transepithelial Cl^- movement. The opening of Cl^- channels in the apical membrane of salivary gland acinar cells initiates the fluid secretion process, whereas the activation of Cl^- channels in both the apical and the basolateral membranes of ductal cells is thought to be necessary for NaCl reabsorption. Different classes of Cl^- channels have been identified in salivary cells, activated by intracellular Ca^{2+}, gated by cAMP, and activated following changes in membrane potential and cell volume. Importantly, only adrenergic response is impaired in most CF exocrine glands, because the secretory portion of CF glands failed to respond to β-adrenergic agonists.

In order to evaluate the effect of GPact-26a *in vivo*, we studied the CFTR-dependent salivary secretion in rat after sub-cutaneous injection of atropine to block the cholinergic dependent secretion (Fig. 7A and B). First, we determined the secretory capacity of saliva by stimulating the salivary glands with GPact-26a alone. GPact-26a at 30 μM by itself did not increase the salivary secretion ($N = 5$). On the contrary, isoprenaline, a β_1- and β_2-adrenoreceptor agonist, at 10 μM, stimulated the salivary secretion ($N = 9$). Addition of GPact-26a to isoprenaline (30 and 10 μM, respectively) increased the collected saliva weights (Fig. 7A and B). Clearly, GPact-26a potentiates the isoprenaline-induced wt-CFTR-dependent salivary secretion in rat ($N = 10$) as observed previously in mice with GPact-11a [30].

2.3. Molecular modelling

In order to delineate potential target sites of the compounds of the GP-family (forty-four compounds: four isomers of GPact-11a, GPinh-5a and **13a**–**21a**) in comparison to the previously described genistein, MBP-104 and IBMX activators [30,39] and $CFTR_{inh}$-172 inhibitor [31,33], we performed *in silico* docking simulations using the homology model of the wt-CFTR outward-facing conformation, made on the basis of the crystal structure of Sav1866 in an outward-facing conformation [11]. This model is assumed to approximate the open form of the channel, at least in the cytoplasmic domains, as the two NDB are tightly associated, with ATP bound at their interfaces. In the first step of simulation, we explored the ability that the selected compounds bind to the cytoplasmic part of the protein excluding thereby the transmembrane helices (TMs) of the membrane spanning domains (MSDs). Both the nucleotide binding domains NBDs (NBD1: residues 386–649, NBD2: 1204–1446) and the intracellular loops (ICLs) of the MSDs constituting the interface between NBDs and MSDs (ICL1: 155–189, ICL2: 255–289, ICL3: 947–980, ICL4: 1048–1082) were conserved. In regard to the large size of the corresponding docking box, the most appropriate software VINA was used in the first step of the docking study with the forty-eight selected compounds performed in the presence of nucleotide (ADP) in both NBDs (Scheme 2).

The first docking calculations showed that all compounds can bind in five different cavities (Fig. 8, Table 1). Two cavities (C1 and C2) are located at the entrance of the nucleotide binding sites occupied by nucleotides. The third identified water-accessible pocket (C3) is located at the opposite face of NBDs–ICLs contact area. The two last cavities (C4, C5) are inner pockets located close to the canonical and non-canonical nucleotide-binding sites, respectively, and delimited in part by ICLs (ICL1,2 and ICL2,3, respectively). All these identified cavities appeared to be located at the nucleotide binding domains interface (NBD1/NBD2).

In the second step of the simulation (Scheme 2), accurate dockings were performed using the VINA, Autodock and GOLD [40,41] software in five small boxes, each ones including one different cavity previously identified. For a same cavity, the three docking software gave similar homogeneous scores with low standard deviations for the affinity of all compounds (data not shown, see in Table 1 the average affinities or scores and the standard deviations calculated for the 48 compounds studied). Thus, the scores obtained for a same cavity appeared to be close for all the GP-family compounds including their four isomers. There was no significant difference between active and non-active compounds including the known modulators. With Autodock and VINA, better homogeneous energies or scores were obtained for the binding of all compounds in the C4 and C5 cavities. With GOLD, the scores in the large inner cavity C4 close to non-canonical ATP binding site jumped about 20% (Table 1) suggesting that cavity C4 could be a preferential possible binding site of GPact-11a and GPact-26a.

Additional docking simulations were performed in each nucleotide binding sites after removal of ADP. In the corresponding

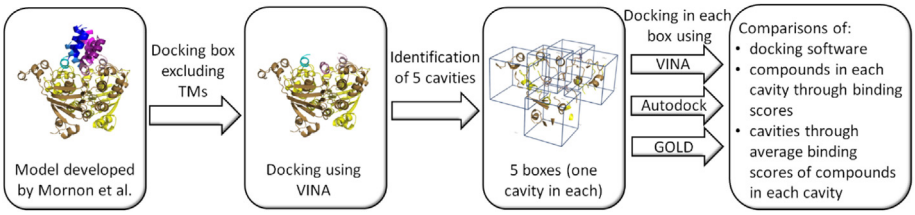

Scheme 2. Method of *in silico* docking used for the delineation of potential targeted sites by the compounds of the GP-family (forty-four compounds: four isomers of GPact-11a, GPinh-5a and **13a**–**21a**) and previously described activators, genistein, MBP-104 and IBMX, and inhibitor $CFTR_{inh}$-172 with the CFTR homology model of the CFTR outward-facing conformation (closed channel) developed by Mornon et al. [11] and the VINA, Autodock and GOLD software. TMs: Transmembrane helices.

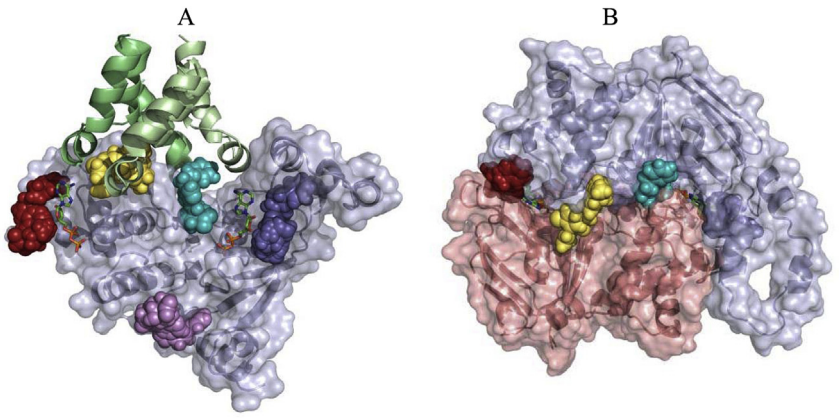

Fig. 8. 3D structure representation of wt-CFTR. The five cavities identified in the presence of ADP (shown as sticks) are shown through coloured volumes: C1, NBD1/NBD2 interface, slate blue; C2, NBD1/NBD2 interface, red; C3, NBD1/NBD2 interface, violet; C4, NBD1/NBD2/ICL1/ICL4 interface, cyan; C5, NBD1/NBD2/ICL2/ICL3 interface, yellow. (A): MSDs: green, NBD1: light blue, NBD2 not drawn; (B): 90° rotation about the *x* axis relative to (A); MSDs not drawn, NBD2: salmon surface. Pictures made with Pymol [50]. (For interpretation of the references to colour in this figure legend, the reader is referred to the web version of this article.)

boxes, the main binding solutions obtained for all selected compounds partly overlap the ADP binding sites and the corresponding scores appeared to be similar to those obtained with the C1–C3 and C5 sites.

3. Discussion and conclusion

In the search for new CFTR modulators, the analogues (**13a**–**21a**) of GPact-11a (**1a**) in which the 9-propyl side chain is modified, were synthesised. Among these analogues, only GPact-26a (**17a**) and the corresponding isomers GPact-26b (**17b**) appeared to be able to strongly activate wt-CFTR at similar concentrations in CHO cells. GPact-26a also activates wt-CFTR in human epithelial MM39 and F508del-CFTR rescued by miglustat in human CF ciliated epithelial cells. GPact-26a was also able to activate wt-CFTR-dependent salivary secretion in rat. It is thus a water-soluble wt-CFTR and F508-del activator in several airway epithelial cell lines as observed *in vitro* (iodide efflux and fluorescence imaging) and *in vivo* (salivary secretion) techniques. GPact-26a showed similar activation properties to those of GPact-11a and, thus, is a good candidate in combination with F508del-CFTR correctors for further developments towards a cystic fibrosis therapy.

From the results obtained with nine analogues of our first lead GPact-11a, it appeared that the possible modifications of the pharmacophoric core at the 9-position are highly limited to the replacement of the 9-propyl chain by a 9-allyl group incorporating the same number of carbon atoms. Introduction at the *N*9 position of shorter and longer side chains led to the loss of activation of wt-type CFTR in CHO cells. Since the presence of 9-isopropyl (**16a**) and 9-propargyl (**19a**) side groups made of three carbon atoms also led to a lack of activity, it can be concluded that (i) the steric hindrance of the hydrophobic group introduced at the 9-position is a key parameter in the activating effect and (ii) this group should be located in a small hydrophobic site of CFTR in which the position of the terminal methyl (GPact-11a) or methylene group (GPact-26a) is crucial for an activation.

The molecular docking study of forty-eight compounds including the GP-family compounds and four known modulators (genistein, MBP-104, IBMX, $CFTR_{inh}$-172) was performed using the homology model of the wt-CFTR outward-facing conformation and the VINA, GOLD and Autodock software. These three software pointed out five main possible binding sites common to the GP compounds and to the four reported modulators studied. These five identified cavities are located at the NBD1/NBD2 interface that is a key feature in the CFTR opening. Accurate dockings in the corresponding boxes did not allow the discrimination between the affinities for a same cavity of the active and non-active compounds. Cavity 4 (NBD1/NBD2/ICL1/ICL4 interface) gave, with the three software used, the better average scores calculated from the scores of the forty eight compounds docked. However, the scores obtained for each compound are high enough to consider a possible binding in the five identified cavities.

These results and the lack of discrimination between active and non-active compounds in the docking study point out the limits of such an *in silico* approach to explain dynamic effects. The observed drastic changes in CFTR activation by modifications of the length and the steric hindrance of the 9-side chain attached to the adenine core cannot be explained at the molecular level through the docking simulations performed. Site-directed mutagenesis experiments especially in cavity 4 are underway in order to determine the CFTR-activating binding cavity of GPact-11a and GPact-26a and to progress in the design of more active activators.

Table 1
Location of the identified binding cavities C1–C5 (NBD: Nucleotide Binding Domain, ICL: intracellular loops) and corresponding average binding energy or fitness score calculated using the VINA, Autodock and GOLD software for the forty-eight compounds studied and standard deviation.

Cavity	C1	C2	C3	C4	C5
Location	NBD1/NBD2	NBD1/NBD2	NBD1/NBD2	NBD1/NBD2/ICL1/ICL4	NBD1/NBD2/ICL2/ICL3
Colour in Fig. 8	slate blue	red	violet	cyan	yellow
Average binding energy and standard deviation (VINA) kcal mol^{-1}	−7.9 ± 0.7	−8.1 ± 0.7	−7.6 ± 0.5	−8.9 ± 0.6	−8.5 ± 0.6
Average binding energy and standard deviation (Autodock) kcal mol^{-1}	−7.7 ± 1.4	−7.7 ± 1.2	−6.9 ± 1.3	−8.6 ± 1.2	−8.3 ± 1.4
Average fitness score and standard deviation (GOLD)	56 ± 5	57 ± 7	55 ± 7	65 ± 7	54 ± 7

4. Experimental

4.1. Chemistry

All starting materials were commercially available research-grade chemicals and used without further purification. Reactions were monitored by analytical TLC on silica gel (Alugram Sil G/UV_{254}) from Macherey–Nagel with fluorescent indicator UV_{254}. Melting points were determined in open glass capillaries using a Büchi 510 apparatus and are reported uncorrected. LRMS were achieved with a NERMAG spectrometer for the FAB, DCI and EI techniques and with a ZQ Waters for the ESI. HRMS and elemental analysis were obtained from the Mass Spectrometry Service, CRMPO, at the University of Rennes I, France, using a Micro-Tof-Q-II Micromass Zabspec-Tof spectrometer for ESI and a Varian Mat311 spectrometer for EI technique, and a Microanalyseur Flash EA1112 CHNS/O Thermo Electron.

^1H and ^{13}C NMR spectra were recorded on a Bruker Avance 400 at 400 MHz and 100 MHz, respectively, using the residual solvent signal as internal standard. Chemical shifts are reported in ppm (parts per million) relative to the residual signal of the solvent, and the signals are described as singlet (s), broad singlet (bs), doublet (d), triplet (t), doublet of doublet (dd), quartet (q), sextuplet (sext), septuplet (sept), multiplet (m); coupling constants are reported in Hertz (Hz). Columns chromatography were performed on silica gel (MN Kieselgel 60, 0.063–0.2 mm/70–230 mesh, Macherey–Nagel) or on C_{18} reversed phase (Macherey–Nagel polygoprep 60–50 C_{18}). HPLC analysis was performed with an Agilent 1100 series using a diode array detector and a C_{18} reversed-phase column (Nucleodur C_{18} ISIS, Macherey–Nagel, 5 μm particle size, 250 mm × 4.6 mm), with a mobile phase composed of A = ammonium acetate 0.1 M pH 7 and B = methanol with a gradient: to 0:100 A:B over 30 min, 1 mL/min, 10 μL injection, detection at 260 nm.

Purity of the evaluated compounds was determined by elemental analysis or HPLC analysis and in every case appeared to be ≥95%.

4.1.1. Synthesis of 9-alkyled adenines

4.1.1.1. General procedure used for preparing 9-alkylated adenine. To a suspension of adenine in dry DMF, NaH (1.1 equiv) was added under argon. The mixture was stirred at rt for 1 h then the alkylating agent (1.05 equiv) was added and the mixture was stirred until complete reaction.

4.1.1.2. Synthesis of 9-isopropyladenine [42] ***5***. After evaporation under reduced pressure, the residue was chromatographed on silica gel eluting with DCM-MeOH giving 9-isopropyladenine **5** as a white solid (457 mg, 2.58 mmol, 26%) obtained from 1.40 g (10.36 mmol) of adenine. ^1H NMR (400 MHz, $CDCl_3$): δ 8.36 (1H, s, CH), 7.88 (1H, s, CH), 5.96 (2H, bs, NH_2), 4.85 (1H, m, CH), 1.61 (6H, d, J = 6.8 Hz, CH_3), ^{13}C NMR (100 MHz, $CDCl_3$): δ 157.7 (C_{IV}), 152.9 (CH_{Ar}), 149.9 (C_{IV}), 138.2 (CH_{Ar}), 120.2 (C_{IV}), 47.2 (CH), 22.9 (CH_3), LRMS (DCI, NH_3, isobutane): calcd for $C_8H_{12}N_5$: $[M + H]^+$ 178, found 178.

4.1.1.3. Synthesis of 9-butyladenine [42] ***6***. After evaporation under reduced pressure, the residue was crystallized from propan-2-ol giving 9-butyladenine **6** as a white solid (9.04 g, 47.28 mmol, 64%) obtained from 10.00 g (74.08 mmol) of adenine. ^1H NMR (400 MHz, $CDCl_3$): δ 8.37 (1H, s, CH), 7.80 (1H, s, CH), 6.34 (2H, bs, NH_2), 4.20 (2H, m, CH_2), 1.89 (2H, m, CH_2), 1.36 (2H, m, CH_2), 0.95 (3H, m, CH_3), ^{13}C NMR (100 MHz, $CDCl_3$): δ 155.4 (C_{IV}), 152.9 (C_{IV}), 140.4 (CH_{Ar}), 129.0 (CH_{Ar}), 119.6 (C_{IV}), 43.7 (CH_2), 32.0 (CH_2), 19.9 (CH_2), 13.5 (CH_3), LRMS (FAB^+, NBA) calcd for $C_9H_{14}N_5$: $[M + H]^+$ 192, found 192.

4.1.1.4. Synthesis of 9-allyladenine [43] ***7***. After evaporation under reduced pressure, the residue was dissolved in 100 mL of aqueous NaOH (1 M) and extracted by 4 × 100 mL of AcOEt. Organic layers are combined, dried and evaporated under reduced pressure. The residue was chromatographed on silica gel eluting with DCM-MeOH giving 9-allyladenine **7** as a white solid (4.06 g, 23.20 mmol, 63%) obtained from 5.00 g (37.04 mmol) of adenine. ^1H NMR (400 MHz, D_2O): δ 7.83 (1H, s, CH_{Ar}), 7.82 (1H, s, CH_{Ar}), 5.89–5.81 (1H, m, CH), 5.11 (1H, d, J = 10.4 Hz, CH_2), 4.88 (1H, d, J = 17.2 Hz, CH_2), 4.54 (2H, dd, J = 1.2 and 4.4 Hz, CH_2), ^{13}C NMR (100 MHz, D_2O): δ 154.8 (C_{IV}), 151.8 (CH_{Ar}), 147.9 (C_{IV}), 141.7 (CH_{Ar}), 131.5 (CH), 117.9 (CH_2), 117.6 (C_{IV}), 45.7 (CH_2), LRMS (FAB^+, glycerol) calcd for $C_8H_{10}N_5$: $[M + H]^+$ 176, found 176.

4.1.1.5. Synthesis of 9-propargyladenine [44] ***8***. After evaporation under reduced pressure, the residue was chromatographed on silica gel eluting with DCM-MeOH giving 9-propargyladenine **8** as a white solid (1.39 g, 8.03 mmol, 67%) obtained from 1.62 g (11.99 mmol) of adenine. ^1H NMR (400 MHz, MeOD): δ 8.24 (1H, s, CH), 8.23 (1H, s, CH), 5.08 (2H, d, J = 2.6 Hz, CH_2), 3.00 (1H, t, J = 2.6 Hz, CH), ^{13}C NMR (100 MHz, MeOD): δ 155.9 (C_{IV}), 152.5 (CH_{Ar}), 148.8 (C_{IV}), 140.5 (CH_{Ar}), 118.6 (C_{IV}), 76.2 (C_{IV}), 74.3 (CH_2), 32.3 (CH). LRMS (FAB^+, glycerol) calcd for $C_8H_8N_5$: $[M + H]^+$ 174, found 174.

4.1.1.6. Synthesis of 9-benzyladenine [42] ***9***. After evaporation under reduced pressure, the residue was dissolved in 100 mL of aqueous NaOH (1 M) and extracted by 4 × 100 mL of DCM. Organic layers are combined, dried and evaporated under reduced pressure. The residue was chromatographed on silica gel eluting with DCM-MeOH giving 9-benzyladenine **9** as a white solid (3.33 g, 14.80 mmol, 40%) obtained from 5.00 g (37.04 mmol) of adenine. ^1H NMR (400 MHz, $CDCl_3$): δ 8.42 (1H, s, CH), 7.78 (1H, s, CH), 7.43–7.28 (5H, m, CH), 5.64 (2H, Bs, NH_2), 5.39 (2H, S, CH_2), ^{13}C NMR (100 MHz, $CDCl_3$): δ 155.6 (C_{IV}), 153.5 (CH_{Ar}), 150.6 (C_{IV}), 140.7 (CH_{Ar}), 135.7 (C_{IV}), 129.3 (CH_{Ar}), 128.7 (CH_{Ar}), 128.0 (CH_{Ar}), 47.5 (CH_2), HRMS (ESI^+) calcd for $C_{12}H_{11}N_5$: $[M]^+$ 225.10145 found 225.1015, $[M-H]^+$ 224.09362 found 224.0947.

4.1.1.7. Synthesis of 9-(3′-phenylpropyl)adenine [45] ***10***. After evaporation under reduced pressure, the residue was crystallized from propan-2-ol giving 9-(3′-phenylpropyl)adenine **10** as a white solid (5.31 g, 20.96 mmol, 57%) obtained from 5.00 g (37.04 mmol) of adenine. ^1H NMR (400 MHz, $CDCl_3$): δ 8.39 (1H, s, CH), 7.76 (1H, s, CH), 7.36–7.14 (5H, m, CH), 5.63 (2H, Bs, NH_2), 4.23 (2H, t, J = 7.2 Hz, CH_2), 2.69 (2H, t, J = 7.2 Hz, CH_2), 2.28 (2H, m, CH_2), ^{13}C NMR (100 MHz, $CDCl_3$): δ 155.5 (C_{IV}), 153.1 (CH_{Ar}), 150.4 (C_{IV}), 140.7 (CH_{Ar}), 140.4 (C_{IV}), 128.8 (CH_{Ar}), 128.6 (CH_{Ar}), 120.0 (C_{IV}), 43.6 (CH_2), 32.9 (CH_2), 31.4 (CH_2), LRMS (ESI^+) calcd for $C_{14}H_{16}N_5$: $[M + H]^+$ 254, found 254.

4.1.1.8. Synthesis of 3-bromo-1-(4′,4″-dimethoxytrityloxy)propane [46]. To a solution of 4,4′-dimethoxytrityl chloride (2.44 g, 7.19 mmol) in pyridine (5 mL), 3-bromopropanol (1.00 g, 0.66 mL) was added. The mixture was stirred at rt during 2 h and then precipitated into MeOH (30 mL). After filtration, the solid was washed with MeOH to give 3-bromopropoxy-DMTr as a white solid (1.97 g, 4.46 mmol, 62%), mp: 85–86 °C. 1H NMR (400 MHz, CDCl3): δ 7.63 (2H, d, J = 7.6 Hz, CH_{Ar}), 7.51 (4H, d, J = 8.8 Hz, CH_{Ar}), 7.42 (1H, t, J = 7.6 Hz, CH_{Ar}), 7.36–7.31 (2H, m, CH_{Ar}), 6.99–6.96 (4H, d, J = 8.8 Hz, CH_{Ar}), 3.85 (6H, s, CH_3), 3.68 (2H, t, J = 6.8 Hz, CH_2), 3.40–3.39 (2H, m, CH_2), 2.24 (2H, m, CH_2), HRMS (EI) calcd for $C_{24}H_{25}O_3^{79}Br$: [M+Na]+ 463.0885, found 463.0884.

*4.1.1.9. Synthesis of 9-[3′-(4″,4‴-dimethoxytrityloxy)propyl]adenine **11**.* After evaporation under reduced pressure, the residue was chromatographed on silica gel eluting with DCM-MeOH. After evaporation under reduced pressure, the residue was crystallized from propan-2-ol giving 9-[3′-(4″,4‴-dimethoxytrityloxy)propyl] adenine **11** as a pale yellow solid (1.26 g, 2.54 mmol, 56%) obtained from 612 mg (4.53 mmol) of adenine, mp: 162–164 °C. ^{1}H NMR (400 MHz, $CDCl_3$): δ 8.39 (1H, s, CH), 7.66 (1H, s, CH), 7.46 (2H, d, J = 7.6 Hz, CH_{Ar}), 7.36–7.26 (7H, m, CH_{Ar}), 6.88 (4H, d, J = 7.6 Hz, CH_{Ar}), 5.88 (2H, bs, NH_2), 4.21 (2H, t, J = 6.4 Hz, CH_2), 3.85 (6H, s, CH_3), 3.18 (2H, t, J = 6.4 Hz, CH_2), 2.12 (2H, t, J = 6.4 Hz, CH_2), ^{13}C NMR (100 MHz, $CDCl_3$): δ 158.7 (C_{IV}), 155.4 (C_{IV}), 152.7 (CH_{Ar}), 150.2 (C_{IV}), 145.0 (C_{IV}), 141.1 (CH_{Ar}), 136.2 (C_{IV}), 130.1 (CH_{Ar}), 128.2 (CH_{Ar}), 128.1 (CH_{Ar}), 127.1 (CH_{Ar}), 119.9 (C_{IV}), 113.3 (CH_{Ar}), 86.3 (C_{IV}), 59.9 (CH_2), 55.4 (CH_3), 41.5 (CH_2), 30.3 (CH_2), HRMS (EI) calcd for $C_{29}H_{30}N_5O_3$: $[M + H]^+$ 496.2349, found 496.2362.

*4.1.1.10. Synthesis of 9-(3′-hydroxypropyl)adenine [42] **12**.* A solution of 9-[3′-(4″,4‴-dimethoxytrityloxy)propyl]adenine **11** (800 mg, 1.61 mmol) in dichloroacetic acid (2% in DCM, 65 mL) was stirred at rt during 1.5 h. The mixture was then neutralized using a saturated solution of $NaHCO_3$. The aqueous layer was evaporated under reduce pressure and the residue was chromatographed on reverse phase (C_{18}) eluting with water-methanol giving 9-(3-hydroxypropyl)-adenine **11** as a white solid (305 mg, 1.58 mmol, 96%), mp: 178–179 °C. ^{1}H NMR (400 MHz, MeOD): δ 8.23 (1H, s, CH), 8.14 (1H, s, CH), 4.37 (2H, t, J = 7.2 Hz, CH_2), 3.57 (2H, t, J = 6.4 Hz, CH_2), 2.09 (2H, m, CH_2), ^{13}C NMR (100 MHz, MeOD): δ 155.9 (C_{IV}), 152.2 (CH_{Ar}), 149.2 (C_{IV}), 141.5 (CH_{Ar}), 57.9 (CH_2), 40.4 (CH_2), 32.0 (CH_2), HRMS (EI) calcd for $C_8H_{11}N_5O$: [M]+ 193.0964, found 193.0970.

4.1.2. Preparation of the adenine methylglyoxal diadducts

4.1.2.1. General procedure used for preparing methylglyoxal adducts. To the commercial concentrated aqueous solution of methylglyoxal (MG) (40%) (8 equiv), the α-aminoazaheterocycle was added. In some cases, the reaction mixture was diluted by addition of water. Argon was flushed through the solution and the mixture was heated at 50 °C until complete reaction under argon. After evaporation under reduced pressure, the residue was chromatographed on Sep-Pak® C18 cartridges (10 g) eluting with H_2O and then H_2O–MeOH (95:5) giving the major isomers adducts **a** except for compound **17**, which for the two isomers were isolated. Compounds **15a**, **17a**, **18a**, and **21a** were also crystallized from propan-2-ol.

*4.1.2.2. Synthesis of 9-methyladenine adducts **13a**.* **13a** (245 mg, 0.80 mmol, 28%) obtained as a pale yellow solid from 450 mg (3.00 mmol) of 9-methyladenine **3** in 40% aqueous solution of MG and 5 mL of water after 24 h at 50 °C, mp: 102–103 °C (dec.). ^{1}H NMR (400 MHz, D_2O): δ 8.31 (1H, s, CH), 8.00 (1H, s, CH), 3.73 (3H, s, CH_3), 1.99 (3H, s, CH_3), 1.54 (3H, s, CH_3), ^{1}H NMR (400 MHz, D_2O, 50 °C): δ 8.63 (1H, s, CH), 8.23 (1H, s, CH), 5.04 (1H, s, CH), 3.95 (3H, s, CH_3), 2.22 (3H, s, CH_3), 1.82 (3H, s, CH_3), ^{13}C NMR (100 MHz, D_2O): δ 177.4 (C_{IV}), 149.4 (C_{IV}), 148.3 (CH_{Ar}), 144.0 (CH_{Ar}), 118.8 (C_{IV}), 82.1 (C_{IV}), 69.9 (CH), 64.8 (C_{IV}), 30.1 (CH_3), 26.7 (CH_3), 21.2 (CH_3), HRMS (EI) calcd for $C_{12}H_{15}N_5O_4$: $[M + H]^+$ 294.1202, found 294.1204, HPLC purity = 96.3%.

*4.1.2.3. Synthesis of 9-ethyladenine adducts **14a**.* **14a** (680 mg, 2.21 mmol, 33%) obtained as a white solid from 1.00 g (6.19 mmol) of 9-ethyladenine **4** in 40% aqueous solution of MG and 15 mL of water after 10 h at 50 °C, mp: 139–141 °C (dec.). ^{1}H NMR (400 MHz, D_2O): δ 8.75 (1H, s, CH), 8.11 (1H, s, CH), 4.42 (1H, s, CH), 4.14 (2H, m, CH_2), 1.63 (3H, s, CH_3), 1.56 (3H, s, CH_3), 1.35 (3H, t, J = 7.2 Hz, CH_3), ^{13}C NMR (100 MHz, D_2O): δ 176.5 (C_{IV}), 146.3 (C_{IV}), 144.4 (CH_{Ar}), 142.6 (CH_{Ar}), 117.4 (C_{IV}), 89.1 (C_{IV}), 70.5 (CH), 63.2 (C_{IV}), 36.7 (CH_2), 25.6 (CH_3), 22.0 (CH_3), 14.4 (CH_3), HRMS (EI) calcd for $C_{13}H_{17}N_5O_4$: $[M + H]^+$ 308.1359,found 308.1359, elemental analysis calcd for $C_{13}H_{17}N_5O_4$, H_2O: C 48.00, H 5.89, N 21.53, found C 47.61, H 5.56, N 21.28.

*4.1.2.4. Synthesis of 9-isopropyladenine adducts **15a**.* **15a** (121 mg, 0.38 mmol, 25%) obtained as a white solid from 250 mg (1.41 mmol) of 9-isopropyladenine **5** in 40% aqueous solution of MG and 3 mL of water after 18 h at 50 °C, mp: 144 °C (dec.). ^{1}H NMR (400 MHz, D_2O): δ 8.77 (1H, s, CH), 8.28 (1H, s, CH), 4.81–4.75 (1H, m, CH), 4.44 (1H, s, CH), 1.61 (3H, s, CH_3), 1.58 (3H, s, CH_3), 1.07 (6H, d, J = 8.4 Hz, 2 CH_3), ^{13}C NMR (100 MHz, D_2O): δ 176.5 (C_{IV}), 146.3 (C_{IV}), 145.1 (C_{IV}), 142.8 (CH_{Ar}), 142.3 (CH_{Ar}), 117.7 (C_{IV}), 89.0 (C_{IV}), 70.5 (CH), 63.2 (C_{IV}), 48.5 (CH), 25.6 (CH_3), 22.1 (CH_3), 21.4 (CH_3), HRMS (EI) calcd for $C_{14}H_{19}N_5O_4$: $[M + H]^+$ 344.1335, found 344.1333, elemental analysis calcd for $C_{14}H_{19}N_5O_4$, Na, ½ C_3H_7OH: C 49.86, H 5.94, N 18.76, found C 49.56, H 6.06, N 18.89.

*4.1.2.5. Synthesis of 9-butyladenine adducts **16a**.* **16a** (432 mg, 1.29 mmol, 11%) obtained as a white solid from 2.50 g (13.07 mmol) of 9-butyladenine **6** in 40% aqueous solution of MG and 5 mL of water after 48 h at 50 °C, mp: 140–142 °C (dec.). ^{1}H NMR (400 MHz, D_2O): δ 8.84 (1H, s, CH), 8.21 (1H, s, CH), 4.53 (1H, s, CH), 4.25 (2H, t, J = 6.8 Hz, CH_2), 1.82 (2H, m, CH_2), 1.74 (3H, s, CH_3), 1.67 (3H, s, CH_3), 1.26 (2H, sext, J = 7.2 Hz, CH_2), 0.87 (3H, t, J = 7.2 Hz, CH_3), ^{13}C NMR (100 MHz, D_2O): δ 175.6 (C_{IV}), 146.5 (C_{IV}), 145.4 (C_{IV}), 144.8 (CH_{Ar}), 142.6 (CH_{Ar}), 117.4 (C_{IV}), 89.1 (C_{IV}), 70.5 (CH), 63.2 (C_{IV}), 44.2 (CH_2), 31.2 (CH_2), 25.5 (CH_3), 22.0 (CH_3), 19.0 (CH_2), 12.6 (CH_3), HRMS (EI) calcd for $C_{15}H_{22}N_5O_4$: $[M + H]^+$ 336.1672, found 336.1683, elemental analysis calcd for $C_{15}H_{21}N_5O_4$, H_2O: C 50.98, H 6.56, N 19.82, found C 51.11, H 6.36, N 19.76.

*4.1.2.6. Synthesis of 9-allyladenine adducts **17a**.* **17a** (1.23 g, 3.86 mmol, 44%) obtained as a white solid from 1.50 g (8.70 mmol) of 9-allyladenine in 40% aqueous solution of MG and 5 mL of water after 12 h at 50 °C, mp: 136–139 °C (dec.). ^{1}H NMR (400 MHz, D_2O): δ 8.81 (1H, s, CH), 8.22 (1H, s, CH), 6.10–6.01 (1H, ddt, J = 17.0, 10.4 and 5.2 Hz, CH), 5.29 (1H, d, J = 10.4 Hz, CH_2), 5.07 (1H, d, J = 17.0 Hz, CH_2), 4.86 (2H, d, J = 5.2 Hz, CH_2), 4.56 (1H, s, CH), 1.75–1.67 (6H, m, CH_3), ^{13}C NMR (100 MHz, D_2O): δ 176.8 (C_{IV}), 146.8 (C_{IV}), 145.3 (C_{IV}), 144.8 (CH_{Ar}), 142.9 (CH_{Ar}), 131.5 (CH), 118.5 (CH_2), 117.5 (C_{IV}), 89.1 (C_{IV}), 70.5 (CH), 63.6 (C_{IV}), 46.3 (CH_2), 25.9 (CH_3), 22.1 (CH_3), LRMS (FAB^+, glycerol) calcd for $C_{14}H_{18}N_5O_4$: $[M + H]^+$ 320, found 320, HPLC purity = 96.3%.

*4.1.2.7. Synthesis of 9-allyladenine adducts **17b**.* **17b** (601 mg, 1.89 mmol, 22%) obtained as a white solid from 1.50 g (8.70 mmol) of 9-allyladenine in 40% aqueous solution of MG and 5 mL of water after 12 h at 50 °C, mp: 143–146 °C (dec.). ^{1}H NMR (400 MHz, D_2O): δ 8.81 (1H, s, CH), 8.25 (1H, s, CH), 6.11–6.01 (1H, ddt, J = 17.0, 10.4 and 5.2 Hz, CH), 5.29 (2H, d, J = 10.4 Hz, CH_2), 5.09 (1H, d, J = 17.0 Hz, CH_2), 4.90 (1H, d, J = 5.2 Hz, CH_2), 4.21 (1H, s, CH), 1.95–1.76 (6H, m, 2 CH_3), ^{13}C NMR (100 MHz, DMSO D_6): δ 175.2 (C_{IV}), 152.2 (C_{IV}), 151.3(C_{IV}), 151.1 (CH_{Ar}), 146.7 (C_{IV}), 141.1 (CH_{Ar}), 131.4 (CH), 118.5 (CH_2), 118.0 (C_{IV}), 73.6 (CH), 65.3 (C_{IV}), 46.4 (CH_2), 24.0 (CH_3), 18.2 (CH_3), HRMS (EI) calcd for $C_{14}H_{18}N_5O_4$: $[M + H]^+$ 320.13588 found 320.1361, HPLC purity = 96.1%.

*4.1.2.8. Synthesis of 9-propargyladenine adducts **18a**.* **18a** (495 mg, 1.56 mmol, 27%) obtained as a pale yellow solid from 1.00 g (5.78 mmol) of 9-propargyladenine in 40% aqueous solution of MG 20 mL of water after 24 h at 50 °C, mp: 147 °C (dec.). ^{1}H NMR (400 MHz, D_2O): δ 8.76 (1H, s, CH), 8.23 (1H, s, CH), 4.98 (2H, s, CH_2),

4.40 (1H, s, CH), 2.82 (1H, s, CH), 1.60 (3H, s, CH_3), 1.55 (3H, s, CH_3), ^{13}C NMR (100 MHz, D_2O): δ 176.2 (C_{IV}), 146.1 (C_{IV}), 145.1 (C_{IV}), 144.0 (CH_{Ar}), 143.0 (CH_{Ar}), 143.0 (C_{IV}), 117.5 (C_{IV}), 98.3 (C_{IV}), 75.6 (CH), 70.4 (CH), 63.3 (C_{IV}), 33.7 (CH_2), 25.5 (CH_3), 22.0 (CH_3), HRMS (EI) calcd for $C_{14}H_{16}N_5O_4$ $[M + H]^+$ 318.1202, found 318.1195, elemental analysis calcd for $C_{14}H_{15}N_5O_4$, Na, ½ C_3H_7OH: C 50.41, H 4.91, N 18.96, found C 50.69, H 4.82, N 19.06.

*4.1.2.9. Synthesis of 9-benzyladenine adducts **19a**.* **19a** (140 mg, 0.35 mmol, 14%) obtained as a pale brown solid from 600 mg (2.67 mmol) of 9-benzyladenine in 40% aqueous solution of MG and 5 mL of water after a week at 50 °C, mp: 170–171 °C (dec.). ^1H NMR (400 MHz, D_2O): δ 8.24 (1H, s, CH), 8.10 (1H, s, CH), 7.30–7.17 (5H, m, 5CH), 5.36 (2H, s, CH_2), 4.89 (1H, s, CH), 2.03 (3H, s, CH_3), 1.53 (3H, s, CH_3), ^{13}C NMR (100 MHz, D_2O): δ 177.5 (C_{IV}), 151.3 (C_{IV}), 147.8 (C_{IV}), 142.5 (CH_{Ar}), 135.7 (C_{IV}), 135.5 (CH_{Ar}), 129.8 (CH_{Ar}), 128.2 (CH_{Ar}), 127.2 (CH_{Ar}), 119.1 (C_{IV}), 98.1 (C_{IV}), 81.1 (CH), 64.8 (C_{IV}), 47.5 (CH_2), 20.2 (CH_3), 12.3 (CH_3), LRMS (ESI^+, glycerol) calcd for $C_{18}H_{20}N_5O_4$: $[M + H]^+$ 370, found 370, HPLC purity = 95.6%.

*4.1.2.10. Synthesis of 9-(3′-phenylpropyl)adenine adducts **20a**.* **20a** (808 mg, 2.11 mmol, 25%) obtained as a white solid from 2.00 g (8.36 mmol) of 9-(3′-phenylpropyl)adenine in 40% aqueous solution of MG and 10 mL of water after 48 h at 50 °C, mp: 149 °C (dec.). ^1H NMR (400 MHz, D_2O): δ 8.11 (1H, s, CH), 7.76 (1H, s, CH), 6.66–6.62 (5H, m, 5CH), 4.80 (1H, s, CH), 4.02 (2H, t, J = 6.6 Hz, CH_2), 2.43 (2H, t, J = 6.6 Hz, CH_2), 2.04 (2H, m, CH_2), 2.00 (3H, s, CH_3), 1.46 (3H, s, CH_3), ^{13}C NMR (100 MHz, D_2O): δ 177.0 (C_{IV}), 151.1 (CH_{Ar}), 149.6 (C_{IV}), 147.2 (C_{IV}), 142.0 (CH_{Ar}), 139.8 (C_{IV}), 127.4 (CH_{Ar}), 127.3 (CH_{Ar}), 125.2 (CH_{Ar}), 118.6 (C_{IV}), 80.1 (CH), 64.4 (C_{IV}), 43.5 (CH_2), 31.8 (CH_2), 28.7 (CH_2), 26.3 (CH_3), 20.2 (CH_3), LRMS (FAB^+, NBA) calcd for $C_{18}H_{20}N_5O_4$: $[M + H]^+$ 398, found 398, elemental analysis calcd for $C_{20}H_{23}N_5O_4$: C 60.44, H 5.83, N 17.62, found C 60.32, H 5.94, N 17.54.

*4.1.2.11. Synthesis of 9-(3′-hydroxypropyl)adenine adducts **21a**.* **21a** (283 mg, 0.84 mmol, 65%) obtained as a white solid from 250 mg (1.29 mmol) of 9-(3′-hydroxypropyl)adenine in 40% aqueous solution of MG and 2 mL of water after 48 h at 50 °C, mp: 103–105 °C (dec.). ^1H NMR (400 MHz, D_2O): δ 8.58 (1H, s, CH), 8.14 (1H, s, CH), 4.72 (1H, s, CH), 4.34 (2H, m, CH_2), 3.57 (2H, m, CH_2), 2.09–2.00 (5H, m, CH_2 and CH_3), 1.72 (3H, s, CH_3), ^1H NMR (400 MHz, D_2O, 45 °C): δ 8.33 (1H, s, CH), 8.13 (1H, s, CH), 4.95 (1H, s, CH), 4.36 (2H, d, J = 7.2 Hz, CH_2), 3.57 (2H, m, CH_2), 2.10 (2H, m, CH_2), 1.91 (3H, s, CH_3), 1.74 (3H, s, CH_3), ^{13}C NMR (100 MHz, D_2O): δ 175.6 (C_{IV}), 152.0 (C_{IV}), 147.9 (CH_{Ar}), 141.8 (CH_{Ar}), 118.8 (C_{IV}), 97.4 (C_{IV}), 79.0 (CH), 63.8 (C_{IV}), 58.0 (CH_2), 40.8 (CH_2), 32.1 (CH_2), 25.7 (CH_3), 20.9 (CH_3), HRMS (EI) calcd for $C_{14}H_{19}N_5O_5$: $[M + H]^+$ 338.1464, found 338.1472,elemental analysis calcd for $C_{14}H_{18}N_5O_5$, Na, ½ H_2O, ½ C_3H_7OH: C 45.31, H 5.51, N 18.22, found C 45.38, H 5.48, N 18.08.

4.2. Biological evaluations

4.2.1. Cell culture

For this study, we used Chinese Hamster Ovary (CHO) cells, stably transfected with pNUT vector containing wild-type CFTR (wt-CFTR CHO). Cells cultured at 37 °C in 5% CO_2 were maintained in αMEM with Glutamax (Invitrogen corporation, USA), containing 7% FCS (BIO-Whittaker Europe, Belgium), 50 IU penicillin/ml (Invitrogen corporation, USA), 50 μg streptomycin/ml (Invitrogen corporation, USA) and 100 μM methotrexate (SIGMA chemicals, USA). The human nasal airway epithelial cell line JME/CF15, derived from a CF patient homozygous for the F508del mutation, was passaged once a week, plated in flasks coated with human placental collagen IV (50 μg/ml, SIGMA chemicals, USA) and cultured in Dulbecco's minimal essential medium/Ham F-12 (3:1) (Invitrogen corporation, USA) supplemented with 10% FCS (BIO-Whittaker Europe, Belgium) and seven growth factors [38]The non CF human tracheal cell line MM39 was also used and cultures as previously described [47].

4.2.2. Iodide efflux

CFTR Cl^- channel activity was assayed on population of cells by the iodide (^{125}I) efflux in the presence of the compounds [48].

Concentration response curves were determined by measuring the rate of iodide (^{125}I) efflux with a high-capacity robotic system (MultiProbe II EXT; PerkinElmer Life and Analytical Sciences, Courtaboeuf, France) adapted to the determination of iodide efflux. The protocol of screening was as follows. CHO cells were cultured in multi-well plates and incubated at 37 °C in Krebs' solution containing 1 μM KI and 1 μCi of $Na^{125}I$/mL (PerkinElmer Life and Analytical Sciences, Boston, MA) during 30 min (CHO cells) to permit the ^{125}I to reach equilibrium. The first three aliquots were used to establish a stable baseline in cold Krebs' buffer (from t_0 to t_2). A medium containing the appropriate compound was then used for the remaining aliquots from t_3 to t_8. Residual radioactivity was extracted at the end of the experiment with a mixture of 0.1 M NaOH and 0.1% SDS and determined using a gamma counter (Cobra II; PerkinElmer Life and Analytical Sciences). The fraction of initial intracellular ^{125}I lost during each time point was determined, and time-dependent rates (k = peak rate, min^{-1}) of ^{125}I efflux were calculated from the following equation: $k = \ln(^{125}I_{t1}/^{125}I_{t2})/(t_1-t_2)$, where $^{125}I_t$ is the intracellular ^{125}I at time t, and t_1 and t_2 are successive time points. Relative rates were calculated as $k_{peak}-k_{basal}$ (min^{-1}), i.e., the maximal value for the time-dependent rate (k_{peak} min^{-1}) excluding the third point used to establish the baseline (k_{basal} min^{-1}). Concentration-dependent activation curves were constructed as a percentage of maximal activation (set at 100%) transformed from the calculated relative rates. CFTR-dependent iodide efflux was stimulated by forskolin.

4.2.3. Cytotoxicity assay for cell survival

Wt-CFTR CHO cells, grown in 96-well plates, were incubated 24 h with different concentrations of drugs. Then, 3-[4,5-dimethylthiazol-2-yl]-2,5diphenyltetrazolium bromide (MTT, 5 mg/ml) (Sigma, USA) was added to the cell medium during 4 h. The absorbance at 570 nm and 630 nm was read. Bars values were calculated from three independent experiments.

4.2.4. Single-cell fluorescence

CFTR activity was assayed by single-cell fluorescence imaging using the potential-sensitive probe, bis(1,3-diethylthiobarbituric acid)trimethine oxonol ($DisBAC_2(3)$), Molecular Probes, Eugene, OR; (for more details see Ref. [37]). The results of fluorescence imaging are presented as transformed data to obtain the percentage signal variation (F_x) relative to the time of addition of the stimulus, according to the equation: $F_x = ([F_t-F_0]/F_0] \times 100$ where F_t and F_0 are the fluorescent values at the time t and at the time of addition of the stimulus, respectively. For histogram representation, the values correspond to the level of stable variation of fluorescence induced by each drug.

4.2.5. Salivary secretion assay

All experiments were performed on male Wistar rats (250–300 g) according to our previous reports [30,38]. Briefly, quiescent rats were maintained in supine orientation with adhesive tape. Subcutaneous injection of GP-act26a was performed in the cheek and saliva was collected with small pieces of Whatman paper inserted in the mouth near to the previously injected cheek. Every 3

or 4 min, a piece of paper was removed and replaced with a second. At the end of the experiment, the net weight of saliva secreted during the collection period was evaluated. For all experiments, basal salivary secretion was inhibited by atropine (1 mM, 50 μL) prior to injection of a saline solution containing atropine (1 mM) mixed with isoprenaline (10 μM), GP-act26a (30 μM) or a mixture isoprenaline (10 μM) + GP-act26a (30 μM). The secretory rate was determined by dividing the weight of sample by the time required for collection in min. The total saliva secretion was determined by addition of all the samples collected during the experiment. These data were then normalized by dividing the result by the weight in grams of the rat.

4.2.6. Data analysis

Data are presented as mean value ± S.E.M, where *n* refers to the number of isolated cell (single cell measurements), cell populations (iodide efflux and cAMP measurements) and N to the number of animals. Sets of data were compared with a Student's *t* test. All graphs are plotted with GraphPad Prism 5.0 for Windows (GraphPad Software, San Diego, CA). Values of $p < 0.05$ were considered as statistically significant: $^{*}p < 0.05$; $^{**}p < 0.01$; $^{***}p < 0.001$. No significant difference was $p > 0.05$.

4.3. Molecular modelling

Docking studies used the modelled structure of human wild type CFTR [11]. The protein 3D structure was prepared using Protein Preparation Wizard module from Schrödinger [49]. All compounds were built and their energies minimized with Schrodinger/MAESTRO [49], using a conjugate gradient method and MMFF94 force field and charges. Exploratory docking was achieved by VINA on a large box of 60 $Å^3$, exhaustiveness parameter was 12 and Energy Range was 5 kcal mol^{-1}. Accurate dockings were achieved using GOLD, VINA and Autodock4 docking software with default parameters, on limited areas selected from former docking. The genetic algorithms of GOLD, VINA and Autodock performed flexible dockings with small molecules while keeping the protein structure rigid. For each compound, 20 poses were generated by VINA and GOLD, 100 by Autodock then ranked according to their binding energy or GOLD-PLP fitness scoring function. Molecular surfaces and docking solutions were analysed with the PYMOL software [50].

Acknowledgements

This work was supported by the French Associations “Vaincre la Mucoviscidose” (BB) and Mucovie (JB) which are gratefully acknowledged.

Appendix A. Supplementary data

Supplementary data related to this article can be found at http://dx.doi.org/10.1016/j.ejmech.2014.06.028.

References

[1] P.B. Davis, M. Drumm, M.W. Konstan, Cystic fibrosis, Am. J. Respir. Crit. Care Med. 154 (1996) 1229–1256.
[2] D.C. Gadsby, Ion channels versus ion pumps: the principal difference, in principle, Nat. Rev. Mol. Cell. Biol. 10 (2009) 344–352.
[3] D.C. Gadsby, P. Vergani, L. Csanady, The ABC protein turned chloride channel whose failure causes cystic fibrosis, Nature 440 (2006) 477–483.
[4] J.R. Riordan, J.M. Rommens, B. Kerem, N. Alon, R. Rozmahel, Z. Grzelczak, J. Zielenski, S. Lok, N. Plavsic, J.L. Chou, et al., Identification of the cystic fibrosis gene: cloning and characterization of complementary DNA, Science 245 (1989) 1066–1073.
[5] J.A. Tabcharani, X.B. Chang, J.R. Riordan, J.W. Hanrahan, Phosphorylation-regulated Cl- channel in CHO cells stably expressing the cystic fibrosis gene, Nature 352 (1991) 628–631.
[6] M.J. Welsh, A.E. Smith, Molecular mechanisms of cftr chloride channel dysfunction in cystic-fibrosis, Cell 73 (1993) 1251–1254.
[7] H.A. Lewis, X. Zhao, C. Wang, J.M. Sauder, I. Rooney, B.W. Noland, D. Lorimer, M.C. Kearins, K. Conners, B. Condon, P.C. Maloney, W.B. Guggino, J.F. Hunt, S. Emtage, Impact of the ΔF508 mutation in first nucleotide-binding domain of human cystic fibrosis transmembrane conductance regulator on domain folding and structure, J. Biol. Chem. 280 (2005) 1346–1353.
[8] A. Szollosi, D.R. Muallem, L. Csanady, P. Vergani, Mutant cycles at CFTR's non-canonical ATP-binding site support little interface separation during gating, J. Gen. Physiol. 137 (2011) 549–562.
[9] J.L. Mendoza, A. Schmidt, P.J. Thomas, Introduction to section IV: biophysical methods to approach CFTR structure, in: M.D. Amaral, K. Kunzelmann (Eds.), Cystic Fibrosis Methods Mol. Biol., Humana Press, 2011, pp. 321–327.
[10] J.P. Mornon, P. Lehn, I. Callebaut, Atomic model of human cystic fibrosis transmembrane conductance regulator: membrane-spanning domains and coupling interfaces, Cell. Mol. Life Sci. 65 (2008) 2594–2612.
[11] J.P. Mornon, P. Lehn, I. Callebaut, Molecular models of the open and closed states of the whole human CFTR protein, Cell. Mol. Life Sci. 66 (2009) 3469–3486.
[12] S. Atwell, C.G. Brouillette, K. Conners, S. Emtage, T. Gheyi, W.B. Guggino, J. Hendle, J.F. Hunt, H.A. Lewis, F. Lu, I.I. Protasevich, L.A. Rodgers, R. Romero, S.R. Wasserman, P.C. Weber, D. Wetmore, F.F. Zhang, X. Zhao, Structures of a minimal human CFTR first nucleotide-binding domain as a monomer, head-to-tail homodimer, and pathogenic mutant, Protein Eng. Des. Sel. 23 (2010) 375–384.
[13] I. Callebaut, R. Eudes, J.P. Mornon, P. Lehn, Nucleotide-binding domains of human cystic fibrosis transmembrane conductance regulator: detailed sequence analysis and three-dimensional modeling of the heterodimer, Cell. Mol. Life Sci. 61 (2004) 230–242.
[14] R. Eudes, P. Lehn, C. Ferec, J.P. Mornon, I. Callebaut, Nucleotide binding domains of human CFTR: a structural classification of critical residues and disease-causing mutations, Cell. Mol. Life Sci. 62 (2005) 2112–2123.
[15] H.A. Lewis, S.G. Buchanan, S.K. Burley, K. Conners, M. Dickey, M. Dorwart, R. Fowler, X. Gao, W.B. Guggino, W.A. Hendrickson, J.F. Hunt, M.C. Kearins, D. Lorimer, P.C. Maloney, K.W. Post, K.R. Rajashankar, M.E. Rutter, J.M. Sauder, S. Shriver, P.H. Thibodeau, P.J. Thomas, M. Zhang, X. Zhao, S. Emtage, Structure of nucleotide-binding domain 1 of the cystic fibrosis transmembrane conductance regulator, EMBO J. 23 (2004) 282–293.
[16] A.W. Serohijos, T. Hegedus, A.A. Aleksandrov, L. He, L. Cui, N.V. Dokholyan, J.R. Riordan, Phenylalanine-508 mediates a cytoplasmic-membrane domain contact in the CFTR 3D structure crucial to assembly and channel function, Proc. Natl. Acad. Sci. U. S. A. 105 (2008) 3256–3261.
[17] D.M. Amaral, M.C. Farinha, Rescuing mutant CFTR: a multi-task approach to a better outcome in treating cystic fibrosis, Curr. Pharm. Des. 19 (2013) 3497–3508.
[18] V. Birault, R. Solari, J. Hanrahan, D.Y. Thomas, Correctors of the basic trafficking defect of the mutant F508del-CFTR that causes cystic fibrosis, Curr. Opin. Chem. Biol. 17 (2013) 353–360.
[19] R.A. Denny, L.K. Gavrin, E. Saiah, Recent developments in targeting protein misfolding diseases, Bioorg. Med. Chem. Lett. 23 (2013) 1935–1944.
[20] A.G. Durmowicz, K.A. Witzmann, C.J. Rosebraugh, B.A. Chowdhury, Change in sweat chloride as a clinical end point in cystic fibrosis clinical trials: the ivacaftor experience, Chest 143 (2013) 14–18.
[21] I. Fajac, I. Sermet-Gaudelus, Cystic fibrosis: new treatments targeting the CFTR protein, Rev. Mal. Respir. 30 (2013) 255–261.
[22] C.M. Farinha, P. Matos, M.D. Amaral, Control of cystic fibrosis transmembrane conductance regulator membrane trafficking: not just from the endoplasmic reticulum to the Golgi, FEBS J. 280 (2013) 4396–4406.
[23] G. Faure, N. Bakouh, N. Odolczyk, H. Xu, F. Saul, G. Planelles, P. Zielenkiewicz, G.L. Lukacs, M. Ollero, A. Edelman, Correcting effect of PLA2 subunit of crotoxin on mutated CFTR: original perspective to investigate the pharmacotherapy of cystic fibrosis, Toxicon 75 (2013) 212.
[24] L.R. Hoffman, B.W. Ramsey, Cystic fibrosis therapeutics: the road ahead, Chest J. 143 (2013) 207–213.
[25] D. Merk, M. Schubert-Zsilavecz, Repairing mutated proteins-development of small molecules targeting defects in the cystic fibrosis transmembrane conductance regulator, Expert Opin. Drug. Discov. 8 (2013) 691–708.
[26] S. Monterisi, V. Casavola, M. Zaccolo, Local modulation of cystic fibrosis conductance regulator: cytoskeleton and compartmentalized cAMP signalling, Br. J. Pharmacol. 169 (2013) 1–9.
[27] E. Nieddu, B. Pollarolo, L. Merello, S. Schenone, M. Mazzei, F508del-CFTR rescue: a matter of cell stress response, Curr. Pharm. Des. 19 (2013) 3476–3496.
[28] T. Ong, B.W. Ramsey, Modifying disease in cystic fibrosis: current and future therapies on the horizon, Curr. Opin. Pulm. Med. 19 (2013) 645–651.
[29] C. Schwarz, Drug therapy for cystic fibrosis, Arzneimitteltherapie 31 (2013) 80–88.
[30] J. Bertrand, B. Boucherle, A. Billet, P. Melin-Heschel, L. Dannhoffer, C. Vandebrouck, C. Jayle, C. Routaboul, M.C. Molina, J.L. Decout, F. Becq, C. Norez, Identification of a novel water-soluble activator of wild-type and F508del CFTR: GPact-11a, Eur. Respir. J. 36 (2010) 311–322.
[31] T.H. Ma, J.R. Thiagarajah, H. Yang, N.D. Sonawane, C. Folli, L.J.V. Galietta, A.S. Verkman, Thiazolidinone CFTR inhibitor identified by high-throughput

screening blocks cholera toxin-induced intestinal fluid secretion, J. Clin. Invest. 110 (2002) 1651–1658.
[32] C. Muanprasat, N.D. Sonawane, D. Salinas, A. Taddei, L.J.V. Galietta, A.S. Verkman, Discovery of glycine hydrazide pore-occluding CFTR inhibitors: mechanism, structure-activity analysis, and in vivo efficacy, J. Gen. Physiol. 124 (2004) 125–137.
[33] C. Routaboul, C. Norez, P. Melin, M.C. Molina, B. Boucherle, F. Bossard, S. Noel, R. Robert, C. Gauthier, F. Becq, J.L. Decout, Discovery of alpha-aminoazaheterocycle-methylglyoxal adducts as a new class of high-affinity inhibitors of cystic fibrosis transmembrane conductance regulator chloride channels, J. Pharmacol. Exp. Ther. 322 (2007) 1023–1035.
[34] C. Routaboul, L. Dumas, I. Gautier-Luneau, J. Vergne, M.C. Maurel, J.L. Decout, New stereoselective reaction of methylglyoxal with 2-aminopyridine and adenine derivatives: formation of imino acid-nucleic base derivatives in water under mild conditions, Chem. Commun. (Camb) (2002) 1114–1115.
[35] B.L. Renard, B. Boucherle, B. Maurin, M.C. Molina, C. Norez, F. Becq, J.L. Decout, An expeditious access to 5-pyrimidinol derivatives from cyclic methylglyoxal diadducts, formation of argpyrimidines under physiological conditions and discovery of new CFTR inhibitors, Eur. J. Med. Chem. 46 (2011) 1935–1941.
[36] O. Moran, O. Zegarra-Moran, On the measurement of the functional properties of the CFTR, J. Cyst. Fibros. 7 (2008) 483–494.
[37] C. Norez, F. Antigny, S. Noel, C. Vandebrouck, F. Becq, A cystic fibrosis respiratory epithelial cell chronically treated by miglustat acquires a non-cystic fibrosis-like phenotype, Am. J. Respir. Cell. Mol. Biol. 41 (2009) 217–225.
[38] S. Noel, C. Faveau, C. Norez, C. Rogier, Y. Mettey, F. Becq, Discovery of pyrrolo [2,3-b]pyrazines derivatives as submicromolar affinity activators of wild type, G551D, and F508del cystic fibrosis transmembrane conductance regulator chloride channels, J. Pharmacol. Exp. Ther. 319 (2006) 349–359.
[39] C. Marivingt-Mounir, C. Norez, R. Derand, L. Bulteau-Pignoux, D. Nguyen-Huy, B. Viossat, G. Morgant, F. Becq, J.-M. Vierfond, Y. Mettey, Synthesis, SAR, crystal structure, and biological evaluation of benzoquinoliziniums as activators of wild-type and mutant cystic fibrosis transmembrane conductance regulator channels, J. Med. Chem. 47 (2004) 962–972.
[40] Gold-Suite in, CCDC, Cambridge, UK.
[41] O. Trott, A.J. Olson, AutoDock Vina: improving the speed and accuracy of docking with a new scoring function, efficient optimization, and multithreading, J. Comput Chem. 31 (2010) 455–461.
[42] C. Lambertucci, I. Antonini, M. Buccioni, D.D. Ben, D.D. Kachare, R. Volpini, K.-N. Klotz, G. Cristalli, 8-Bromo-9-alkyl adenine derivatives as tools for developing new adenosine A2A and A2B receptors ligands, Bioorg. Med. Chem. 17 (2009) 2812–2822.
[43] J. Thibon, L. Latxague, G. Deleris, Synthesis of silicon analogues of acyclonucleotides incorporable in oligonucleotide solid-phase synthesis, J. Org. Chem. 62 (1997) 4635–4642.
[44] W. Edward Lindsell, C. Murray, P.N. Preston, T.A.J. Woodman, Synthesis of 1,3-diynes in the purine, pyrimidine, 1,3,5-triazine and acridine series, Tetrahedron 56 (2000) 1233–1245.
[45] V.I. Petrov, A.A. Ozerov, M.S. Novikov, C. Pannecouque, J. Balzarini, E. De Clercq, 9-(2-Aryloxyethyl) derivatives of adenine – a new class of non-nucleosidic antiviral agents, Chem. Heterocycl. Compd. 39 (2003) 1218–1226.
[46] M. Nielsen, A.H. Thomsen, E. Clo, F. Kirpekar, K.V. Gothelf, Synthesis of linear and tripoidal oligo(phenylene ethynylene)-based building blocks for application in modular DNA-programmed assembly, J. Org. Chem. 69 (2004) 2240–2250.
[47] M.D. Merten, W. Kammouni, W. Renaud, F. Birg, M.G. Mattei, C. Figarella, A transformed human tracheal gland cell line, MM-39, that retains serous secretory functions, Am. J. Respir. Cell. Mol. Biol. 15 (1996) 520–528.
[48] C. Norez, G.D. Heda, T. Jensen, I. Kogan, L.K. Hughes, C. Auzanneau, R. Derand, L. Bulteau-Pignoux, C. Li, M. Ramjeesingh, H. Li, D.N. Sheppard, C.E. Bear, J.R. Riordan, F. Becq, Determination of CFTR chloride channel activity and pharmacology using radiotracer flux methods, J. Cyst. Fibros. 3 (2004) 119–121.
[49] Maestro, in, Schrödinger LLC.
[50] PyMOL Molecular Graphics System, in, Schrödinger, LLC.